FUNDAMENTAL LIMITS ON LOCALIZATION IN SINGLE INPUT MULTIPLE OUTPUT VISIBLE LIGHT SYSTEMS

A THESIS SUBMITTED TO

THE GRADUATE SCHOOL OF ENGINEERING AND SCIENCE

OF BILKENT UNIVERSITY

IN PARTIAL FULFILLMENT OF THE REQUIREMENTS FOR

THE DEGREE OF

MASTER OF SCIENCE

IN

ELECTRICAL AND ELECTRONICS ENGINEERING

By

Furkan Kökdoğan

September 2017

Fundamental Limits on Localization in Single Input Multiple Output Visible Light Systems
By Furkan Kökdoğan
September 2017

We certify that we have read this thesis and that in our opinion it is fully adequate, in scope and in quality, as a thesis for the degree of Master of Science.

Sinan Gezici(Advisor)

Orhan Arıkan

Çağatay Candan

Approved for the Graduate School of Engineering and Science:

Ezhan Karaşan
Director of the Graduate School

ABSTRACT

FUNDAMENTAL LIMITS ON LOCALIZATION IN SINGLE INPUT MULTIPLE OUTPUT VISIBLE LIGHT SYSTEMS

Furkan Kökdoğan
M.S. in Electrical and Electronics Engineering
Advisor: Sinan Gezici
September 2017

Visible light systems have recently been considered as an effective and promising solution for indoor positioning. In this thesis, a theoretical accuracy analysis is conducted for position estimation in visible light systems based on received signal strength (RSS) measurements. Considering a single light emitting diode (LED) at the transmitter and multiple photo-detectors (PDs) at the receiver, the Cramér-Rao lower bound (CRLB) is derived for both a generic three-dimensional scenario and specific configurations of the PDs at the receiver. For the special case in which the height of the receiver is known, a compact expression is derived for the CRLB, considering a uniform circular layout and the same elevation angle for all the PDs. Asymptotic analysis and accuracy of derived compact expression is investigated for this configuration of the system. In addition, the optimal placement of the PDs at the receiver is investigated by taking the effects of the elevation angle parameter of the PDs into consideration. The optimal values are obtained theoretically and also verified by simulations. Numerical examples are presented to illustrate the impacts of system parameters on localization accuracy, namely radius of the uniform circular layout, elevation angle and number of PDs. Finally, theoretical limits are compared against the maximum likelihood estimator (MLE) as a benchmark to evaluate the performance of receiver position estimation.

Keywords: Cramér-Rao lower bound, estimation, visible light, positioning, single input multiple output (SIMO), Lambertian pattern, received signal strength, maximum likelihood estimator.

ÖZET

TEK GİRDİLİ ÇOK ÇIKTILI GÖRÜNÜR IŞIK SİSTEMLERİ İLE KONUMLANDIRMADA TEMEL LİMİTLER

Furkan Kökdoğan
Elektronik Mühendisliği, Yüksek Lisans
Tez Danışmanı: Sinan Gezici
Eylül 2017

Görünür ışık sistemleri son zamanlarda kapalı mekanlarda konumlandırma için etkili ve gelecek vaat eden bir çözüm olarak görülmektedir. Bu tezde, görünür ışık sistemleri ile, alınan sinyal gücü ölçümlerine dayanarak yapılan konumlandırmada kuramsal bir doğruluk analizi ortaya konmaktadır. Vericide tek bir ışık saçan diyot (LED), alıcıda ise birden fazla ışık dedektörü (PD) olduğu düşünülerek, hem genel bir üç boyutlu senaryo için hem de ışık dedektörlerinin alıcı üzerindeki özel kurguları için Cramer-Rao alt sınırı türetilmektedir. Alıcı yüksekliğinin bilindiği özel bir kurgu için Cramer-Rao alt sınırı kesif bir ifade olarak türetilmektedir. Bu özel kurguda ışık dedektörleri çembersel bir tasarımda aynı eğim açıları ile dizilmektedir. Bu kurgu için türetilen kesif ifadenin yanaşık analizi ve doğruluğu araştırılmaktadır. Ayrıca ışık dedektörlerinin eğim açıları göz önüne alınarak, alıcı üzerindeki en uygun yerleşimleri araştırılmaktadır. En uygun değerler kuramsal olarak bulunmakta ve benzetimlerle doğrulanmaktadır. Sistem parametrelerinin konumlandırma doğruluğundaki etkilerini göstermek için sayısal örnekler sunulmaktadır. Bu parametreler, çembersel tasarımın yarıçapı, ışık dedektörlerinin eğim açısı ve sayısıdır. Son olarak, kuramsal limitler konum kestiriminin performansını değerlendirebilmek amacıyla en yüksek olabilirlik kestiricisi ile karşılaştırılmaktadır.

Anahtar sözcükler: Cramer-Rao alt sınırı, kestirim, görünür ışık, konumlandırma, tek girdili çok çıktılı, Lambert modeli, alınan sinyal gücü, en yüksek olabilirlik kestiricisi.

Acknowledgement

First of all, I would like to present my sincere thanks to my advisor Assoc. Prof. Sinan Gezici for his guidance, support and supervision throughout this work. It is an extraordinary privilege and a great honor for me to work with him as he is an inspiring and very successful yet modest and benevolent academician. I could not wish a better advisor for my M.S. studies. I believe it would not be possible for me to achieve this thesis without his endless support.

I would also like to thank Prof. Orhan Arıkan and Prof. Çağatay Candan for accepting to be in the thesis committee and examining my thesis.

I would like to thank my family, my mother Havva, my father Faruk, my brother Yasin, my sister Betül and my girlfriend Nagehan for their love, support and encouragement. I would not have had the motivation to achieve this work if they were not always there for me.

I would also like to thank my friend Osman Erdem for his valuable contributions.

Finally, I would also like to thank The Scientific and Technological Research Council of Turkey (TÜBİTAK) for the financial support through BİDEB 2210-A Scholarship Program during my study.

Contents

1 Introduction **1**

1.1 Related Work 3

1.2 Thesis Overview 5

2 System Model **7**

3 CRLB Derivations and Receiver Design **9**

3.1 Known Height and Perpendicular PDs 11

3.2 Known Height, Identical PDs, Equal Noise Variances, and Uniform Circular Layout 12

3.3 Known Height, Perpendicular and Identical PDs, Equal Noise Variances, and Uniform Circular Layout 19

4 Numerical Results **26**

4.1 Accuracy of Asymptotic Results 27

4.2 Uniform Circular Layouts with Various Radii 29

4.3 Elevated PDs at VLC Receiver 30

4.4 Number of PDs and Layout Radius 32

4.5 Maximum Likelihood Estimator (MLE) 34

5 Concluding Remarks and Future Work **36**

List of Figures

1.1 Examples of visible light communication and positioning systems. 2

2.1 SIMO VLP system. 8

3.1 Uniform circular layout. (a) Three-dimensional view. (b) Top view. 13

4.1 The approximate CRLB expressions compared with the exact CRLB. (a) Accuracy of Lemma 1 and Lemma 2. (b) Accuracy of Corollary 1 and Corollary 2. 28

4.2 Three different scenarios with 12 PDs pointing up vertically and 3 circles with different radii. 29

4.3 CRLB versus distance from the room center. 30

4.4 CRLB contour with respect to β and distance from the room center. 31

4.5 CRLB versus N for various radii. 33

4.6 RMSE of MLE versus CRLB for different β values. 35

List of Tables

3.1 List of trigonometric summations for ψ_n in (3.20). 25

Chapter 1

Introduction

Wireless indoor localization has been a popular research and development area in both academic and industrial communities [1]– [4]. Since the Global Positioning System (GPS) cannot provide high localization accuracy for indoor environments [5, 6], various radio-frequency (RF) based solutions, such as WiFi and ultra-wideband (UWB) systems, are developed for indoor localization [1, 2, 7, 8]. As an alternative to RF based localization, light emitting diode (LED) based visible light positioning (VLP) systems are proposed and investigated in recent studies [9]. Accurate position information can be obtained via VLP systems since a line-of-sight path is commonly present and significantly stronger than multipath components in a visible light channel. In addition, visible light systems can simultaneously be used for illumination and data communication, as well [10, 11].

In a visible light system, LEDs are used as transmitters and photodetectors (PDs) can be employed as receivers. LEDs have high modulation bandwidth, on the order of MHz, as opposed to the conventional lighting sources [12]. This enables data transmission while illuminating an indoor environment since human eye averages out the received power from an LED and cannot recognize the blinking at high frequencies. Using LEDs for illumination purposes has some advantages as well. LEDs consume less power and have higher lifetime than traditional light bulbs. Therefore, conventional lighting sources are being replaced

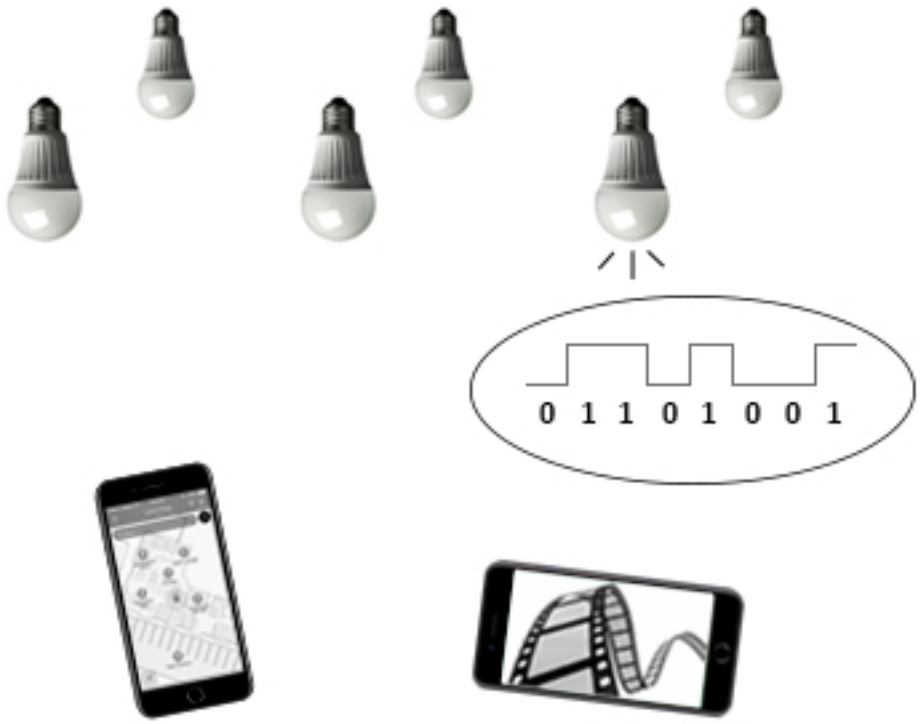

Figure 1.1: Examples of visible light communication and positioning systems.

by LEDs rapidly which facilitates the utilization of visible light communication and positioning systems [13]. At the receiver in a visible light system, a simple PD circuit can be used to measure the received optical power. For communication purposes a single LED and a single PD is sufficient. An LED can be modulated to transmit the data and the receiver circuit can demodulate it as depicted in Fig. 1.1. For VLP systems however, multiple LEDs or multiple PDs are required to achieve a diversity to estimate the location of the receiver.

There are several potential applications of VLP. First, a VLP system can be utilized for location aware content transmission. This for example suits the scenario of a museum where the visitors are informed about the artwork they stand in front of. Another possible application would be the tracking of valuable assets, e.g. biomedical instruments in a hospital [9]. Robot navigation is also a

significant problem which can be solved via VLP systems efficiently. As another example, utilization of VLP can make the automatic management of large warehouses containing many different products possible. Finally, a VLP system can also serve as an indoor navigation assistant for visually impaired people [9].

1.1 Related Work

Position estimation in VLP systems can be performed by utilizing different types of parameters such as received signal strength (RSS), time-of-arrival (TOA), time-difference-of-arrival (TDOA), and angle-of-arrival (AOA). RSS based VLP systems rely on estimating the position of a visible light communication (VLC) receiver based on RSS measurements at the receiver related to a number of LED transmitters [14]– [19]. The study in [15] uses RSS measurements for accurate positioning of devices with light sensing capabilities by utilizing existing LED lamps as transmitters and performing trilateration. Particle filtering based position tracking is proposed in [14], where the position is estimated via RSS measurements. In [18], the basic-framed slotted ALOHA (BFSA) protocol is employed in a VLC based indoor positioning system which uses RSS information for estimating positions of VLC receivers. The study in [19] proposes a carrier allocation VLC system utilizing the intensity modulation and direct detection (IM/DD) method and reports centimeter level positioning accuracies through experimental studies. In addition to the RSS parameter, the TOA and TDOA parameters are also used for position estimation in the literature [20, 21]. In [21], an indoor VLP system that employs TDOA measurements from three LED transmitters is proposed for two-dimensional positioning. The use of the AOA parameter is also considered for position estimation in VLP systems [22]– [24]. In addition, [25] investigates a hybrid positioning system that utilizes both AOA and RSS information, where the position estimation is performed via a weighted least squares estimator.

The topic of this thesis is on RSS based VLP in the presence of a single LED

transmitter and multiple photo-detectors (PDs) at the receiver, which can be regarded as a single input multiple output (SIMO) system. In the literature, there exist some studies on SIMO VLP systems such as [16, 23, 26]. In [16], a VLP system consisting of a single LED transmitter and multiple (three) optical receivers is designed, and the position of the receiver unit is estimated based on RSS measurements and the relative positions among the receivers. The study in [23] investigates the use of both AOA and RSS information for three-dimensional positioning in an indoor localization scenario with a single LED transmitter and multiple tilted optical receivers. The three-dimensional position is estimated based on the gain differences among the tilted PDs, which are functions of both the AOA and the RSS. In [26], an aperture-based angular diversity receiver is proposed for a VLP system which employs a receiver with multiple elements, each consisting of an aperture and a PD. The RSS measurements at the PDs are used to estimate the position of the receiver and the Cramér-Rao lower bound (CRLB) is calculated for the considered model. Multiple transmitter and/or receiver elements are also considered for visible light *communication* (VLC) systems and advantages in terms of data rate and capacity are investigated [27, 28]. For example, [28] proposes novel angle diversity receiver designs, called pyramid receiver and hemispheric receiver, for multiple input multiple output (MIMO) VLC systems and analyzes the effects of the PD elevation angle on the channel capacity.

To provide benchmarks for VLP algorithms in the literature and to illustrate the effects of system parameters on localization performance, theoretical accuracy limits are obtained in various recent studies such as [20, 25, 26], [29]– [34]. In [29], the CRLB is derived for distance estimation based on RSS measurements in a visible light system, and its dependence on system parameters, such as the signal bandwidth, LED configuration, and transmitter height, is investigated. The study in [20] presents the CRLB on TOA based distance estimation in a synchronous VLC system, and analyzes the effects of various system parameters, such as the area of the photo detector, source optical power, and center frequency, on the estimation accuracy. In [30], the CRLBs and maximum likelihood estimators (MLEs) are obtained for synchronous and asynchronous VLP systems, and hybrid TOA/RSS based distance estimation is proposed, which utilizes both the

time delay parameter and the channel attenuation factor. Also, comparisons are provided based on the analytical CRLB expressions for TOA based, RSS based, and hybrid TOA/RSS based distance estimation. The study in [25], which focuses on AOA and RSS based three-dimensional localization, derives a CRLB expression for RSS based three-dimensional localization for a generic deployment scenario. In [34], direct and two-step positioning approaches are investigated for synchronous and asynchronous VLP systems and CRLB expressions are derived for generic configurations. As an alternative to the CRLB, [32] and [33] focus on the Ziv-Zakai bound (ZZB) for distance estimation in asynchronous and synchronous VLP systems, respectively. In particular, [32] derives the ZZB in RSS based VLP systems and provides comparisons with the maximum a-posteriori probability (MAP) and the minimum mean-squared error (MMSE) estimators.

1.2 Thesis Overview

In this thesis, theoretical accuracy limits, namely, CRLB expressions, are obtained for SIMO VLP systems based on RSS measurements. First, a generic three-dimensional localization scenario is considered, and then specific configurations of the PDs at the receiver are considered. For the case with a known receiver height and a uniform circular layout for the PDs (which is a common and efficient configuration, as investigated in [28]), a compact CRLB expression is derived, which is used to obtain asymptotic CRLB expressions when the radius of the circular layout is significantly smaller (or, larger) than the distance between the receiver and the projection of the LED transmitter to the floor. In addition, guidelines are provided regarding the optimal placement of the PDs at the receiver based on the CRLB expressions. Furthermore, the CRLB expressions are compared against the MLE for the receiver position. The main contributions and the novelty of the thesis can be summarized as follows:

- The CRLB is derived for a generic three-dimensional SIMO VLP for the first time in the literature. (The study in [26] presents a CRLB expression for a system employing multiple PDs (each with aperture) at the receiver

by considering a two-dimensional scenario (i.e., known receiver height) and perpendicular PDs at the receiver.)

- A new compact CRLB expression is obtained when the receiver is at a known height with identical PDs arranged in a uniform circular layout (see Fig. 3.1). In addition, asymptotic CRLB expressions are obtained in this scenario for different system configurations (Lemma 1 and Lemma 2).
- Under certain conditions, it is proved that it is optimal (in terms of CRLB minimization) to place the PDs to the maximum possible radius in the uniform circular layout (Section 3.3, Proposition 1).
- The MLE for the SIMO VLP system is derived and its performance is compared against the CRLB.

In addition, various numerical examples are presented to investigate the effects of system parameters, such as the elevation angles of PDs, layout radius, and number of PDs, on localization accuracy.

The rest of the thesis is organized as follows: The system model is described in Chapter 2. The CRLB expressions in the generic three-dimensional scenario and the special cases with a known receiver height are obtained in Chapter 3, which also includes asymptotic CRLB expressions and guidelines for optimal placement of PDs. Chapter 4 presents simulation results and discussions, and Chapter 5 concludes the thesis with remarks and future work directions.

Chapter 2

System Model

Consider a SIMO VLP system as illustrated in Fig. 2.1, where the transmitter consists of a single LED and the VLC receiver consists of N PDs. The location of the LED is represented by a three-dimensional column vector denoted as $\boldsymbol{l}_T$, which is known by the VLC receiver. (In practice, the LED can periodically broadcast its location information.) The unknown location of the VLC receiver is represented by $\boldsymbol{l}_R$ and the location of the nth PD in the VLC receiver is denoted by $\boldsymbol{l}_R+\boldsymbol{a}_n$. The vectors $\boldsymbol{a}_n$ are known parameters which can be adjusted according to the layout design in the system. Based on the Lambertian formula, the RSS observation (measurement) at the nth PD can be expressed as [27]

$$P_{R_n} = \frac{m+1}{2\pi} P_T \cos^m(\phi_n) \cos(\theta_n) \frac{S_n}{d_n^2} \mathbb{I}_{\{\theta_n \leq \theta_{\mathrm{FOV},n}\}} + \eta_n \tag{2.1}$$

for $n \in \{1, \ldots, N\}$, where m is the Lambertian order of the LED, P_T is the transmit power, S_n is area of the nth PD, ϕ_n is the irradiation angle with respect to the nth PD, θ_n is the incidence angle for the nth PD, $\theta_{\mathrm{FOV},n}$ is the field of view (FOV) of the nth PD, $\mathbb{I}_{\{\cdot\}}$ denotes the indicator function, d_n is the distance between the nth PD and the LED, and η_n is the measurement noise at the nth PD, which is modeled by a zero mean Gaussian random variable with variance σ_n^2 [25]. It is assumed that the measurement noise η_n is independent across different PDs. Also, distance d_n between the nth PD and the LED can be expressed as

$$d_n = \|\boldsymbol{l}_R + \boldsymbol{a}_n - \boldsymbol{l}_T\|. \tag{2.2}$$

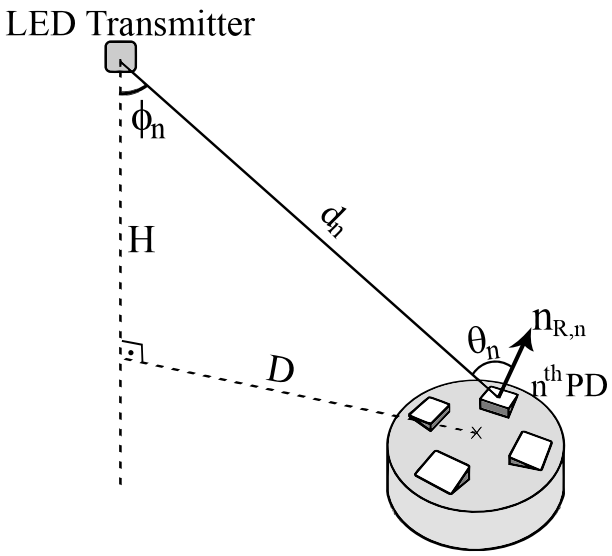

Figure 2.1: SIMO VLP system.

Let $\mathbf{n}_{R,n}$ denote the normal vector for the nth PD, as shown in Fig. 2.1. Then, the cosine of the incidence angle for the nth PD is given by

$$\cos(\theta_n) = \frac{\mathbf{n}_{R,n}^T(\boldsymbol{l}_T - \boldsymbol{l}_R - \boldsymbol{a}_n)}{d_n}. \tag{2.3}$$

Assuming that the LED is above the VLC receiver and faces downwards with the normal vector $\mathbf{n}_T = [0\ 0\ -1]^T$, the cosine of the irradiation angle is obtained as

$$\cos(\phi_n) = \frac{l_T(3) - l_R(3) - a_n(3)}{d_n} \tag{2.4}$$

where $l_T(3)$, $l_R(3)$, and $a_n(3)$ represent the third elements of $\boldsymbol{l}_T$, $\boldsymbol{l}_R$, and $\boldsymbol{a}_n$, respectively. It is noted that the assumption leading to (2.4) is valid in most practical scenarios since LEDs are commonly inserted at the ceiling of a room and face downwards to have efficient illumination [20, 24, 29].

Chapter 3

CRLB Derivations and Receiver Design

In this section, a generic CRLB expression is derived for the SIMO VLP system, and specific expressions are obtained under special cases. Then, optimum placement of PDs in a VLC receiver is considered for uniform circular layouts.

Let $\boldsymbol{P}_R$ represent a vector consisting of the RSS observations at the PDs; that is, $\boldsymbol{P}_R = [P_{R_1} \cdots P_{R_N}]^T$, where P_{R_n} is as in (2.1). The aim is to estimate the location of the VLC receiver, $\boldsymbol{l}_R$, based on $\boldsymbol{P}_R$. To calculate the CRLB for this estimation problem, the probability density function (PDF) of $\boldsymbol{P}_R$ conditioned on $\boldsymbol{l}_R$ can be obtained from (2.1) as follows:

$$p(\boldsymbol{P}_R|\boldsymbol{l}_R) = \left(\prod_{n=1}^{N} \frac{1}{\sqrt{2\pi}\sigma_n}\right) \exp\left\{-\sum_{n=1}^{N} \frac{(P_{R_n} - f_n(\boldsymbol{l}_R))^2}{2\sigma_n^2}\right\} \tag{3.1}$$

with

$$f_n(\boldsymbol{l}_R) \triangleq \frac{(m+1)P_T \cos^m(\phi_n)\cos(\theta_n)S_n}{2\pi d_n^2} \tag{3.2}$$

where it is assumed that the LED is in the FOV of all the PDs. From (2.3) and (2.4), $f_n(\boldsymbol{l}_R)$ in (3.2) can be specified as

$$f_n(\boldsymbol{l}_R) = \frac{P_T(m+1)S_n(l_T(3) - l_R(3) - a_n(3))^m}{2\pi\|\boldsymbol{l}_T - \boldsymbol{l}_R - \boldsymbol{a}_n\|^{m+3}} \mathbf{n}_{R,n}^T(\boldsymbol{l}_T - \boldsymbol{l}_R - \boldsymbol{a}_n)\,. \tag{3.3}$$

The CRLB provides a lower limit on mean-squared errors (MSEs) of unbiased estimators. For the considered SIMO VLP system, the CRLB for estimating the location of the VLC receiver can be stated as follows:

$$\mathbb{E}\big\{\big\|\hat{\boldsymbol{l}}_R - \boldsymbol{l}_R\big\|^2\big\} \geq \text{trace}\big\{\boldsymbol{J}(\boldsymbol{l}_R)^{-1}\big\} \triangleq CRLB \tag{3.4}$$

where $\hat{\boldsymbol{l}}_R$ is an unbiased estimate of $\boldsymbol{l}_R$ and $\boldsymbol{J}(\boldsymbol{l}_R)$ is the Fisher information matrix (FIM) given by

$$\boldsymbol{J}(\boldsymbol{l}_R) = \mathbb{E}\{(\nabla_{\boldsymbol{l}_R} \log p(\boldsymbol{P}_R|\boldsymbol{l}_R))(\nabla_{\boldsymbol{l}_R} \log p(\boldsymbol{P}_R|\boldsymbol{l}_R))^T\} \tag{3.5}$$

with $\nabla_{\boldsymbol{l}_R}$ denoting the gradient operator with respect to $\boldsymbol{l}_R$ [35].

From (3.1), the elements of the FIM in (3.5) can be calculated after some manipulation as

$$[\boldsymbol{J}(\boldsymbol{l}_R)]_{ij} = \sum_{n=1}^{N} \frac{1}{\sigma_n^2} \frac{\partial f_n(\boldsymbol{l}_R)}{\partial l_R(i)} \frac{\partial f_n(\boldsymbol{l}_R)}{\partial l_R(j)} \tag{3.6}$$

for $i, j \in \{1, 2, 3\}$, where $f_n(\boldsymbol{l}_R)$ is as in (3.3) and $l_R(i)$ denotes the ith element of $\boldsymbol{l}_R$. Based on (3.3), the partial derivatives in (3.6) can be obtained as follows:

$$\frac{\partial(f_n(\boldsymbol{l}_R))}{\partial l_R(1)} = c_n(l_T(3) - l_R(3) - a_n(3))^m \frac{-\text{n}_{R,n}(1)d_n^2 + (m+3)u_n(1)\mathbf{n}_{R,n}^T\boldsymbol{u}_n}{d_n^{m+5}} \tag{3.7}$$

$$\frac{\partial(f_n(\boldsymbol{l}_R))}{\partial l_R(2)} = c_n(l_T(3) - l_R(3) - a_n(3))^m \frac{-\text{n}_{R,n}(2)d_n^2 + (m+3)u_n(2)\mathbf{n}_{R,n}^T\boldsymbol{u}_n}{d_n^{m+5}} \tag{3.8}$$

$$\begin{aligned}\frac{\partial(f_n(\boldsymbol{l}_R))}{\partial l_R(3)} &= c_n(l_T(3) - l_R(3) - a_n(3))^m \frac{-\text{n}_{R,n}(3)d_n^2 + (m+3)u_n(3)\mathbf{n}_{R,n}^T\boldsymbol{u}_n}{d_n^{m+5}} \\ &\quad - c_n m(u_n(3))^{m-1}\mathbf{n}_{R,n}^T\boldsymbol{u}_n d_n^{-m-3}\end{aligned} \tag{3.9}$$

where

$$c_n \triangleq \frac{(m+1)P_T S_n}{2\pi} \quad \text{and} \quad \boldsymbol{u}_n \triangleq \boldsymbol{l}_T - \boldsymbol{l}_R - \boldsymbol{a}_n \tag{3.10}$$

with $\text{n}_{R,n}(i)$ and $u_n(i)$ denoting the ith elements of $\mathbf{n}_{R,n}$ and $\boldsymbol{u}_n$, respectively.

The FIM in (3.5) can be evaluated via (3.6)–(3.10), and the CRLB for the SIMO VLP system can be calculated from (3.4). The provided CRLB expression

can be employed to evaluate performance of practical SIMO VLP systems. It is noted that the CRLB expression specified by (3.4)–(3.10) is generic for any configuration and orientation of the PDs at the VLC receiver and is valid for three-dimensional scenarios. Such a CRLB expression has not been available for SIMO VLP systems in the literature. In the following sections, some special cases of the CRLB expression are investigated.

3.1 Known Height and Perpendicular PDs

Consider a scenario in which the height of the VLC receiver, $l_R(3)$, is known and the PDs point upwards such that $\mathbf{n}_{R,n} = [0\ 0\ 1]^T$ and $a_n(3) = 0$ for $n = 1, \ldots, N$. In other words, all the PDs are at the same known height and point up vertically. Such a scenario can, for example, be encountered in robotic applications where the VLC receiver is mounted on the top of a robot that has a known height [9].

In this scenario, $f_n(\boldsymbol{l}_R)$ in (3.3) reduces to the following:

$$f_n(\boldsymbol{l}_R) = \frac{(m+1)P_T S_n (l_T(3) - l_R(3))^{m+1}}{2\pi \|\boldsymbol{l}_T - \boldsymbol{l}_R - \boldsymbol{a}_n\|^{m+3}} \,. \tag{3.11}$$

Then, the 2×2 FIM can be obtained based on $[\boldsymbol{J}(\boldsymbol{l}_R)]_{ij}$ in (3.6) for $i, j \in \{1, 2\}$ as follows:[1]

$$\boldsymbol{J}(\boldsymbol{l}_R) = \begin{bmatrix} J_{11} & J_{12} \\ J_{21} & J_{22} \end{bmatrix} \tag{3.12}$$

where

$$J_{11} = \underbrace{\alpha \sum_{n=1}^{N} \frac{S_n^2}{\sigma_n^2} \frac{(l_{R_n}(1) - l_T(1))^2}{||\boldsymbol{l}_{Rn} - \boldsymbol{l}_T||^{2m+10}}}_{\beta_1} \,, \tag{3.13}$$

$$J_{22} = \underbrace{\alpha \sum_{n=1}^{N} \frac{S_n^2}{\sigma_n^2} \frac{(l_{R_n}(2) - l_T(2))^2}{||\boldsymbol{l}_{Rn} - \boldsymbol{l}_T||^{2m+10}}}_{\beta_2} \,, \tag{3.14}$$

[1] Since the height is known, there exist only two unknowns, $\boldsymbol{l}_R(1)$ and $\boldsymbol{l}_R(2)$, in this scenario.

$$J_{12} = J_{21} = \alpha \underbrace{\sum_{n=1}^{N} \frac{S_n^2}{\sigma_n^2} \frac{(l_{R_n}(1) - l_T(1))(l_{R_n}(2) - l_T(2))}{||\boldsymbol{l}_{Rn} - \boldsymbol{l}_T||^{2m+10}}}_{\gamma} \tag{3.15}$$

with

$$\begin{aligned} \boldsymbol{l}_{Rn} &\triangleq \boldsymbol{l}_R + \boldsymbol{a}_n, \\ l_{R_n}(i) &\triangleq l_R(i) + a_n(i) \\ \alpha &\triangleq \frac{(m+1)^2}{4\pi^2} P_T^2 (m+3)^2 (l_T(3) - l_R(3))^{2m+2}. \end{aligned} \tag{3.16}$$

From (3.12)–(3.15), the CRLB in (3.4) can be calculated in closed form as

$$CRLB = \frac{\beta_1 + \beta_2}{\alpha(\beta_1 \beta_2 - \gamma^2)} \tag{3.17}$$

where β_1, β_2, and γ are as defined in (3.13)–(3.15). Based on (3.17), the CRLB can easily be evaluated for various scenarios in which the PDs are at the same known height and point up vertically.

3.2 Known Height, Identical PDs, Equal Noise Variances, and Uniform Circular Layout

A common configuration for PDs at a VLC receiver is the uniform circular layout, as investigated in [28]. In this section, the PDs are assumed to be identical in the sense that they have equal areas; that is, $S_n = S$ for $n = 1, \ldots, N$, and the noise variances are modeled to be the same; i.e., $\sigma_n^2 = \sigma^2$ for $n = 1, \ldots, N$. In addition, it is assumed that all the PDs are at the same known height, tilted with the same angle β, and are placed in a uniform circular layout, as illustrated in Fig. 3.1-(a). (The motivations for this configuration can be found in [28].) It is noted that if $\beta \in (0, \pi/2)$, the PDs face outwards with respect to the circular layout and if $\beta \in (-\pi/2, 0)$, the PDs face inwards.

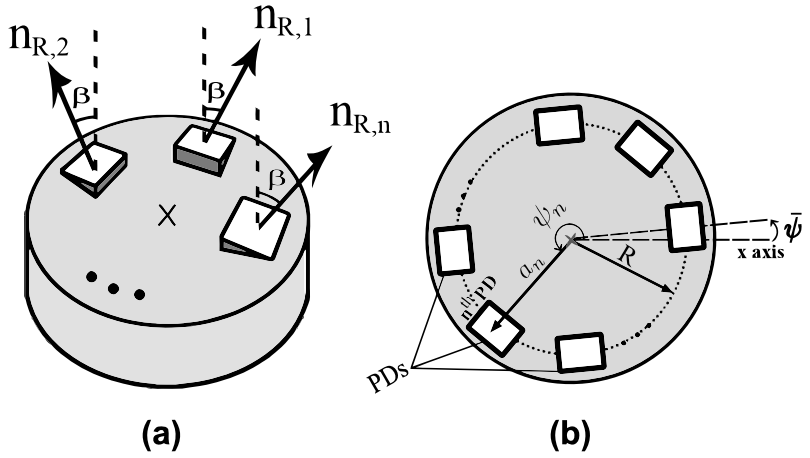

Figure 3.1: Uniform circular layout. (a) Three-dimensional view. (b) Top view.

In this scenario, the radius of the circular layout is represented by R, and the height difference between the LED and the VLC receiver is denoted by H; that is,

$$l_T(3) - l_R(3) = H. \tag{3.18}$$

In addition, the elements of $\boldsymbol{a}_n$ can be written as

$$\begin{aligned} a_n(1) &= R\cos\psi_n, \\ a_n(2) &= R\sin\psi_n, \\ a_n(3) &= 0, \end{aligned} \tag{3.19}$$

for $n = 1, \ldots, N$, with

$$\psi_n \triangleq \frac{2\pi(n-1)}{N} + \bar{\psi} \tag{3.20}$$

where $\bar{\psi}$ is a random shift angle with $0 \leq \bar{\psi} < 2\pi/N$ (see Fig. 3.1-(b)). Then, the distance between the LED and the nth PD can be expressed, from (3.18) and (3.19), as

$$d_n = \|\boldsymbol{l}_R + \boldsymbol{a}_n - \boldsymbol{l}_T\| = \sqrt{(d_x + R\cos\psi_n)^2 + (d_y + R\sin\psi_n)^2 + H^2} \tag{3.21}$$

where d_x, d_y and D (see Fig. 2.1) are defined as

$$d_x \triangleq l_R(1) - l_T(1), \tag{3.22}$$

$$d_y \triangleq l_R(2) - l_T(2), \tag{3.23}$$

$$D \triangleq \sqrt{d_x^2 + d_y^2}\,. \tag{3.24}$$

Also, the normal vectors for each PD can be expressed as

$$\begin{aligned} \mathbf{n}_{R,n}(1) &= \sin\beta\cos\psi_n, \\ \mathbf{n}_{R,n}(2) &= \sin\beta\sin\psi_n, \\ \mathbf{n}_{R,n}(3) &= \cos\beta. \end{aligned} \tag{3.25}$$

Based on the specifications/definitions in (3.18)–(3.25), the elements of the FIM can be obtained from (3.6)–(3.10) as follows:

$$J_{11} = \tilde{a}\sum_{n=1}^{N} A_n^2 \tag{3.26}$$

$$J_{22} = \tilde{a}\sum_{n=1}^{N} B_n^2 \tag{3.27}$$

$$J_{12} = J_{21} = \tilde{a}\sum_{n=1}^{N} A_n B_n \tag{3.28}$$

where

$$\tilde{a} \triangleq \frac{(m+1)^2 P_T^2 S^2 H^{2m}}{4\pi^2\sigma^2} \tag{3.29}$$

$$\begin{aligned} A_n \triangleq\ & \frac{-\sin\beta\cos\psi_n}{d_n^{m+3}} \\ & + (m+3)u_n(1)\frac{\sin\beta\cos\psi_n u_n(1) + \sin\beta\sin\psi_n u_n(2) + \cos\beta u_n(3)}{d_n^{m+5}} \end{aligned} \tag{3.30}$$

$$\begin{aligned} B_n \triangleq\ & \frac{-\sin\beta\sin\psi_n}{d_n^{m+3}} \\ & + (m+3)u_n(2)\frac{\sin\beta\cos\psi_n u_n(1) + \sin\beta\sin\psi_n u_n(2) + \cos\beta u_n(3)}{d_n^{m+5}}\,. \end{aligned} \tag{3.31}$$

Then, the CRLB in (3.4) can be obtained as

$$CRLB = \frac{\frac{1}{\tilde{a}} \sum_{n=1}^{N} (A_n^2 + B_n^2)}{\sum_{n=1}^{N} A_n^2 \sum_{n=1}^{N} B_n^2 - \left(\sum_{n=1}^{N} A_n B_n \right)^2} \cdot \tag{3.32}$$

In order to provide simple approximate expressions for the CRLB in this scenario, the following results are presented.

Lemma 1: *As $D/R \longrightarrow 0$, the CRLB in* (3.32) *can be approximated as*

$$CRLB \approx \frac{2}{J_{11}} \tag{3.33}$$

where J_{11} is given by

$$\begin{aligned} J_{11} = \frac{\tilde{c}}{2} N \big[& (H^2 + R^2)^2 \sin^2 \beta - 2(H^2 + R^2)(m+3) R \sin \beta \, (R \sin \beta - H \cos \beta) \\ & + (m+3)^2 R^2 \left(R^2 \sin^2 \beta + H^2 \cos^2 \beta - HR \sin 2\beta \right) \big] \end{aligned} \tag{3.34}$$

with

$$\tilde{c} \triangleq \frac{(m+1)^2 P_T^2 S^2 H^{2m}}{4\pi^2 \sigma^2 (H^2 + R^2)^{m+5}} \cdot \tag{3.35}$$

Proof: As $D/R \rightarrow 0$, the distance from the LED to each PD becomes approximately $d_n \approx \sqrt{H^2 + R^2} = d$. Also, $u_n(1)$ and $u_n(2)$ can be approximated as

$$\begin{aligned} u_n(1) &\approx -R \cos \psi_n, \\ u_n(2) &\approx -R \sin \psi_n. \end{aligned} \tag{3.36}$$

Then, substituting d_n, $u_n(1)$ and $u_n(2)$ into (3.30), J_{11} in (3.26) can be stated after some manipulation as

$$\begin{aligned} J_{11} = \tilde{c} \sum_{n=1}^{N} \big(& d^4 \sin^2 \beta \cos^2 \psi_n - 2d^2 \sin^2 \beta (m+3) R^2 \cos^4 \psi_n \\ & + 2d^2 \sin^2 \beta (m+3) R^2 \cos^2 \psi_n \sin^2 \psi_n + d^2 \sin 2\beta (m+3) \\ & \times HR \cos^2 \psi_n + (m+3)^2 \sin^2 \beta R^4 \cos^6 \psi_n + (m+3)^2 \\ & \times \sin^2 \beta R^4 \cos^2 \psi_n \sin^4 \psi_n + (m+3)^2 \cos^2 \beta H^2 R^2 \cos^2 \psi_n \\ & + 2(m+3)^2 \sin^2 \beta R^4 \cos^4 \psi_n \sin^2 \psi_n - (m+3)^2 \sin 2\beta \\ & \times HR^3 \cos^4 \psi_n - (m+3)^2 \sin 2\beta HR^3 \cos^2 \psi_n \sin^2 \psi_n \;) \end{aligned} \tag{3.37}$$

where $\tilde{c}$ is defined as

$$\tilde{c} \triangleq \frac{\tilde{a}}{(H^2+R^2)^{m+5}} \tag{3.38}$$

with $\tilde{a}$ being as in (3.29). The expression in (3.37) can also be stated as

$$\begin{aligned}
J_{11} = \tilde{c}\Bigg(& d^4 \sin^2\beta \sum_{n=1}^{N} \cos^2\psi_n \\
& - 2d^2 \sin^2\beta(m+3)R^2 \sum_{n=1}^{N} \cos^4\psi_n \\
& + 2d^2 \sin^2\beta(m+3)R^2 \sum_{n=1}^{N} \cos^2\psi_n \sin^2\psi_n \\
& + d^2 \sin 2\beta(m+3)HR \sum_{n=1}^{N} \cos^2\psi_n \\
& + (m+3)^2 \sin^2\beta R^4 \sum_{n=1}^{N} \cos^6\psi_n \\
& + (m+3)^2 \sin^2\beta R^4 \sum_{n=1}^{N} \cos^2\psi_n \sin^4\psi_n \\
& + (m+3)^2 \cos^2\beta H^2 R^2 \sum_{n=1}^{N} \cos^2\psi_n \\
& + 2(m+3)^2 \sin^2\beta R^4 \sum_{n=1}^{N} \cos^4\psi_n \sin^2\psi_n \\
& - (m+3)^2 \sin 2\beta HR^3 \sum_{n=1}^{N} \cos^4\psi_n \\
& - (m+3)^2 \sin 2\beta HR^3 \sum_{n=1}^{N} \cos^2\psi_n \sin^2\psi_n \Bigg).
\end{aligned} \tag{3.39}$$

From (3.20), the summation terms in (3.39) can be calculated as shown in Table 3.1. Then, reorganizing the terms and substituting the value of d (i.e., $\sqrt{H^2+R^2}$) into (3.39), J_{11} is obtained as in (3.34).

Based on a similar approach, the other elements of the FIM can be obtained as

$$J_{22} = J_{11} \tag{3.40}$$

$$J_{12} = J_{21} = 0\,. \tag{3.41}$$

From (3.40) and (3.41), the CRLB can be obtained via (3.4) as

$$CRLB = \frac{J_{11} + J_{22}}{J_{11}J_{22} - (J_{12})^2} = \frac{2}{J_{11}} \cdot \tag{3.42}$$

Therefore, for $D \ll R$, the CRLB can be approximated as in (3.33), where J_{11} is given by (3.34). ■

Lemma 2: *As $R/D \longrightarrow 0$, the CRLB in* (3.32) *can be approximated as*

$$CRLB \approx \frac{J_{11} + J_{22}}{J_{11}J_{22} - J_{12}J_{21}} \tag{3.43}$$

where J_{11}, J_{22}, J_{12}, and J_{21} are given by (3.44)–(3.46).

$$\begin{aligned} J_{11} = \frac{\bar{c}}{8} N \big[& 4d^4 \sin^2\beta - 8d^2 \sin^2\beta (m+3)({d_x}^2 + R^2) + 4d^2 \sin(2\beta)(m+3)HR \\ & + \sin^2\beta (m+3)^2 \big[4\left({d_x}^4 + {d_x}^2 {d_y}^2 + R^4\right) + R^2\left(27{d_x}^2 + {d_y}^2\right) \big] \\ & - 4\sin(2\beta)(m+3)^2 HR\left(4{d_x}^2 + R^2\right) + 4\cos^2\beta (m+3)^2 H^2\left(2{d_x}^2 + R^2\right) \big] \end{aligned} \tag{3.44}$$

$$\begin{aligned} J_{22} = \frac{\bar{c}}{8} N \big[& 4d^4 \sin^2\beta - 8d^2 \sin^2\beta (m+3)({d_y}^2 + R^2) + 4d^2 \sin(2\beta)(m+3)HR \\ & + \sin^2\beta (m+3)^2 \big[4\left({d_y}^4 + {d_y}^2 {d_x}^2 + R^4\right) + R^2\left(27{d_y}^2 + {d_x}^2\right) \big] \\ & - 4\sin(2\beta)(m+3)^2 HR\left(4{d_y}^2 + R^2\right) + 4\cos^2\beta (m+3)^2 H^2\left(2{d_y}^2 + R^2\right) \big] \end{aligned} \tag{3.45}$$

$$\begin{aligned} J_{12} = J_{21} = \frac{\bar{c}}{4}(m+3) N d_x d_y \big[& \sin^2\beta \left((m+3)\left(13R^2 + 2D^2\right) - 4d^2\right) \\ & - 8\sin(2\beta)H(m+3)R + 4\cos^2\beta (m+3)H^2 \big] \end{aligned} \tag{3.46}$$

Proof: As $R/D \to 0$, the distance from the LED to each PD can be approximated as $d_n \approx \sqrt{H^2 + D^2} \triangleq d$. Substituting the exact values of $u_n(1)$ and $u_n(2)$ (see (3.10)) into (3.30), the first element of the FIM in (3.26) can be calculated

after some manipulation as

$$
\begin{aligned}
J_{11} = \bar{c}\sum_{n=1}^{N} \big(& d^4 \sin^2\beta \cos^2\psi_n - 2d^2 \sin^2\beta(m+3)\cos^2\psi_n \\
& \times (d_x - R\cos\psi_n) - 2d^2 \sin^2\beta(m+3)\cos\psi_n \sin\psi_n \\
& \times (d_x - R\cos\psi_n)(d_y - R\sin\psi_n) - d^2 \sin 2\beta(m+3)H \\
& \times \cos\psi_n (d_x - R\cos\psi_n) + (m+3)^2 \sin^2\beta\cos^2\psi_n \\
& \times (d_x - R\cos\psi_n)^4 + (m+3)^2 \sin^2\beta \sin^2\psi_n (d_x - R\cos\psi_n)^2 \\
& \times (d_y - R\sin\psi_n)^2 + (m+3)^2 \cos^2\beta H^2 (d_x - R\cos\psi_n)^2 \\
& + 2(m+3)^2 \sin^2\beta\cos\psi_n \sin\psi_n (d_x - R\cos\psi_n)^3 \\
& \times (d_y - R\sin\psi_n) + (m+3)^2 \sin 2\beta H \cos\psi_n (d_x - R\cos\psi_n)^3 \\
& + (m+3)^2 \sin 2\beta H \sin\psi_n (d_x - R\cos\psi_n)^2 (d_y - R\sin\psi_n) \ )
\end{aligned} \tag{3.47}
$$

where

$$
\bar{c} \triangleq \frac{\tilde{a}}{(H^2 + D^2)^{m+5}} \tag{3.48}
$$

with $\tilde{a}$ being as in (3.29). From (3.20), the summation terms in (3.47) can be calculated as specified in Table 3.1. Then, reorganizing the terms and substituting the value of d (i.e., $\sqrt{H^2 + D^2}$) into (3.47), J_{11} can be simplified to the expression in (3.44). Following a similar approach, the remaining elements of the FIM can be obtained as in (3.45) and (3.46). Then, for $D \gg R$, the CRLB can be found as in (3.43). ■

For scenarios with known receiver heights, identical PDs and uniform circular layouts, Lemma 1 and Lemma 2 provide approximate closed-form expressions for the CRLB when the horizontal distance between the LED and the center of the receiver is significantly larger or significantly smaller than the radius of the circular layout, respectively. In other words, the CRLB expression in Lemma 1 is expected to be accurate when the receiver is directly under the LED whereas that in Lemma 2 becomes accurate as the receiver is located away from the projection of the LED onto the $x - y$ plane (i.e., the floor).

3.3 Known Height, Perpendicular and Identical PDs, Equal Noise Variances, and Uniform Circular Layout

In this section, it is assumed that all the PDs are identical, at the same known height, point up vertically, and are placed in a uniform circular layout (similar to [20,24,29]). Since this scenario is a special case of the scenario in the previous section for $\beta = 0$ (see Fig. 3.1), the exact CRLB expression can still be calculated from (3.32) by simplifying the definitions of A_n and B_n in (3.30) and (3.31) as

$$A_n \triangleq \frac{(m+3)u_n(1)u_n(3)}{d_n^{m+5}}\,, \tag{3.49}$$

$$B_n \triangleq \frac{(m+3)u_n(2)u_n(3)}{d_n^{m+5}}\,. \tag{3.50}$$

In addition, the results in Lemma 1 and Lemma 2 can be employed to obtain simple approximate expressions for the CRLB in this case.

Corollary 1: *When all the PDs point up vertically, the CRLB in* (3.32) *multiplied by* $R^2/(H^2+R^2)^{m+5}$ *has the following limit as* $D/R \longrightarrow 0$*:*

$$\lim_{\frac{D}{R}\to 0} \frac{R^2 CRLB}{(H^2+R^2)^{m+5}} = \frac{16\pi^2\sigma^2}{S^2(m+1)^2(m+3)^2P_T^2H^{2m+2}N}\,. \tag{3.51}$$

Proof: As $D/R \longrightarrow 0$, the CRLB in (3.32) converges to the CRLB expression specified by (3.33) and (3.34) in Lemma 1. When all the PDs point up vertically, i.e., when $\beta = 0$, J_{11} in (3.34) becomes

$$J_{11} = \frac{\tilde{c}}{2}(m+3)^2H^2R^2N\,. \tag{3.52}$$

Then, the CRLB in (3.33) is obtained as

$$CRLB = \frac{4}{\tilde{c}(m+3)^2H^2R^2N}\,. \tag{3.53}$$

Inserting the definition of $\tilde{c}$ in (3.35) into (3.53), the following CRLB expression is obtained for $D/R \longrightarrow 0$:

$$CRLB = \frac{16\pi^2\sigma^2(H^2+R^2)^{m+5}}{S^2(m+1)^2(m+3)^2P_T^2H^{2m+2}NR^2}\,. \tag{3.54}$$

Therefore, as $D/R \longrightarrow 0$, the limit of the CRLB in (3.54) multiplied by $R^2/(H^2+R^2)^{(m+5)}$ can be obtained as specified in (3.51). ■

Based on (3.51) in Corollary 1, the CRLB can be approximated for $D \ll R$ as

$$CRLB \approx \frac{16\pi^2\sigma^2(H^2+R^2)^{m+5}}{S^2(m+1)^2(m+3)^2P_T^2H^{2m+2}NR^2}\,. \tag{3.55}$$

It is noted that the CRLB in meters (i.e., the square-root of (3.55)) is inversely proportional to the transmit power, the area of the PDs, and the square-root of the number of PDs in this configuration. By calculating the first-order derivative, it can be shown that the CRLB in (3.55) is a monotone decreasing function of R if

$$(H/R)^2 > m+4 \tag{3.56}$$

and is monotone increasing otherwise. For common room dimensions and VLC receiver layouts, H/R is expected to be larger than 10 when the LED transmitter is on the ceiling. Therefore, the condition in (3.56) is satisfied in most practical scenarios as the Lambertian order, m, cannot be very large unless the LED is very directive (which is not very desirable due to illumination purposes). Hence, in the case of $D \ll R$ and practical system parameters, *the PDs should be placed at the boundary of the uniform circular layout to minimize the CRLB.*

Corollary 2: *When all the PDs point up vertically, the CRLB in* (3.32) *multiplied by* $R^2/(H^2+D^2)^{m+5}$ *has the following limit as* $R/D \longrightarrow 0$*:*

$$\lim_{\frac{R}{D}\to 0}\frac{R^2CRLB}{(H^2+D^2)^{m+5}} = \frac{8\pi^2\sigma^2}{S^2(m+1)^2(m+3)^2P_T^2H^{2m+2}N}\,. \tag{3.57}$$

Proof: As $R/D \longrightarrow 0$, the CRLB in (3.32) converges to the CRLB expression specified by (3.43) and (3.44)–(3.46) in Lemma 2. When all the PDs point up vertically, i.e., when $\beta = 0$, the elements of the FIM in (3.44)–(3.46) reduce to the following expressions:

$$J_{11} = \frac{\bar{c}}{2}(m+3)^2H^2N(2d_x^2+R^2) \tag{3.58}$$

$$J_{22} = \frac{\bar{c}}{2}(m+3)^2H^2N(2d_y^2+R^2) \tag{3.59}$$

$$J_{12} = J_{21} = \bar{c}(m+3)^2H^2Nd_xd_y\,. \tag{3.60}$$

Evaluating (3.43) for this scenario, the CRLB becomes

$$CRLB = \frac{4(D^2+R^2)}{\bar{c}(m+3)^2H^2R^2N(2D^2+R^2)}\,. \tag{3.61}$$

Inserting the definition of $\bar{c}$ in (3.48) into (3.61), the following CRLB expression is obtained for $R/D \longrightarrow 0$:

$$CRLB = \frac{4(D^2+R^2)(H^2+D^2)^{m+5}}{\tilde{a}(m+3)^2H^2R^2N(2D^2+R^2)}\,. \tag{3.62}$$

As $R/D \longrightarrow 0$, the limit of the CRLB in (3.62) multiplied by $R^2/(H^2+D^2)^{m+5}$ becomes

$$\begin{aligned}\lim_{\frac{R}{D}\to 0}\frac{R^2CRLB}{(H^2+D^2)^{m+5}} &= \frac{4}{\tilde{a}(m+3)^2H^2N}\lim_{\frac{R}{D}\to 0}\frac{(D^2+R^2)}{(2D^2+R^2)}\\ &= \frac{2}{\tilde{a}(m+3)^2H^2N}\,.\end{aligned} \tag{3.63}$$

Then, based on the definition of $\tilde{a}$ in (3.29), the statement in (3.57) can be obtained from (3.63). ■

For $D \gg R$, the CRLB can be approximated from (3.57) in Corollary 2 as

$$CRLB \approx \frac{8\pi^2\sigma^2(H^2+D^2)^{m+5}}{S^2(m+1)^2(m+3)^2P_T^2H^{2m+2}NR^2}\,. \tag{3.64}$$

It is again noted that the CRLB in meters (i.e., the square-root of (3.64)) is inversely proportional to the transmit power, the area of the PDs, and the square-root of the number of PDs in this configuration. Another important property of the CRLB in (3.64) is its monotone decreasing nature with respect to the radius of the uniform circular layout. Hence, *the PDs should be placed at the boundary of the uniform circular layout to achieve the minimum CRLB in this scenario.*

Remark 1: Considering practical receiver sizes and room dimensions, the case of $D \gg R$ is expected to be quite common in real-life applications. Hence, the expressions in Lemma 2 and Corollary 2 hold approximately in most scenarios under the stated conditions. On the other hand, the case of $R \gg D$ considered in Lemma 1 and Corollary 1 can be observed when the VLC receiver is directly under the LED transmitter; i.e., when D in Fig. 2.1 is very small. The accuracy of the proposed expressions is investigated in the next section (see Fig. 4.1).

As noted in Remark 1, the case of $D \gg R$ is quite common in practical applications; hence, the expression is (3.64) can provide a simple approximate expression for the CRLB in the case of a uniform circular layout and perpendicular and identical PDs that are at the same known height. Since the CRLB in (3.64) decreases with R, it is optimal to place the PDs at the boundary of the uniform circular layout (as stated after Corollary 2). In order to generalize this result to more generic configurations, the following proposition is presented.

Proposition 1: *Consider a configuration that is a superposition of multiple circular uniform arrays as in Fig. 4.2-(a), and suppose that the PDs are identical, at the same known height, and point up vertically. Then, for $D \gg R$, the radii of all the circles should be set to the maximum possible value in order to minimize the CRLB.*

Proof: Consider a layout that is a superposition of K circles with different radii denoted by $R_1, R_2, \ldots, R_K$, and let N_k represent the number of uniformly located PDs at the kth circle. In this case, the total number of PDs, denoted by N, becomes

$$N = \sum_{k=1}^{K} N_k \,. \tag{3.65}$$

Under the conditions in the proposition, J_{11} in (3.13) can be expressed via (3.21) as

$$J_{11} = \alpha \sum_{n=1}^{N} \frac{S^2}{\sigma^2} \frac{(l_R(1) - l_T(1) + a_n(1))^2}{(d_n)^{m+5}} \tag{3.66}$$

$$= \tilde{\alpha} \sum_{k=1}^{K} \sum_{i=1}^{N_k} \frac{(l_R(1) - l_T(1) + a_{k,i}(1))^2}{(d_{k,i})^{m+5}} \tag{3.67}$$

where $d_{k,i}$ denotes the distance between the LED and the ith PD at the kth circle, $a_{k,i}(1)$ represents the first coordinate of the difference between the receiver location ($\boldsymbol{l}_R$) and the location of the ith PD at the kth circle, α is as in (3.1), and $\tilde{\alpha}$ is defined as

$$\tilde{\alpha} \triangleq \frac{\alpha S^2}{\sigma^2} \,. \tag{3.68}$$

Similar to (3.19), $a_{k,i}(1)$, $a_{k,i}(2)$, and $a_{k,i}(3)$ can be expressed as

$$\begin{aligned} a_{k,i}(1) &= R_k \cos\psi_{k,i}, \\ a_{k,i}(2) &= R_k \sin\psi_{k,i}, \\ a_{k,i}(3) &= 0, \end{aligned} \tag{3.69}$$

where $\psi_{k,i}$ is the angle of the ith PD at the kth circle with respect to the x-axis; that is (cf. (3.20)),

$$\psi_{k,i} = \frac{2\pi\,(i-1)}{N_k} + \bar{\psi}_k \tag{3.70}$$

with $\bar{\psi}_k$ denoting the random shift angle for the kth circle (see Fig. 3.1-(b)).

From $a_{k,i}(1)$ in (3.69), the definitions of d_x and D in (3.22) and (3.24), respectively, and based on the assumption of $d_{k,l} \approx \sqrt{H^2 + D^2}$ (since $D \gg R$), J_{11} in (3.67) can be written in the following form:

$$J_{11} = \tilde{\alpha} \sum_{k=1}^{K} \sum_{i=1}^{N_k} \frac{d_x^2 + 2d_x R_k \cos\psi_{k,i} + R_n^2 \cos^2\psi_{k,i}}{(D^2+H^2)^{m+5}} \tag{3.71}$$

which can also be expressed as

$$J_{11} = \hat{c}\left(N d_x^2 + 2d_x \sum_{k=1}^{K} R_k \sum_{i=1}^{N_k} \cos\psi_{k,i} + \sum_{k=1}^{K} R_k^2 \sum_{i=1}^{N_k} \cos^2\psi_{k,i} \right) \tag{3.72}$$

where

$$\hat{c} \triangleq \frac{\tilde{\alpha}}{(H^2+D^2)^{m+5}}\,. \tag{3.73}$$

From Table 3.1, the elements in (3.72) can be calculated as

$$\begin{aligned} \sum_{i=1}^{N_k} \cos\psi_{k,i} &= \sum_{i=1}^{N_k} \cos\left(\frac{2\pi(i-1)}{N_k} + \bar{\psi}_k \right) = 0 \\ \sum_{i=1}^{N_k} \cos^2\psi_{k,i} &= \sum_{i=1}^{N_k} \cos^2\left(\frac{2\pi(i-1)}{N_k} + \bar{\psi}_k \right) = \frac{N_k}{2}\,. \end{aligned}$$

Then, J_{11} in (3.72) can be simplified to

$$J_{11} = \hat{c}\left(N d_x^2 + \frac{1}{2} \sum_{k=1}^{K} R_k^2 N_k^2 \right). \tag{3.74}$$

Via similar calculations, the other elements of the FIM in (3.14) and (3.15) are obtained as

$$J_{22} = \hat{c}\left(Nd_y^2 + \frac{1}{2}\sum_{k=1}^{K} R_k^2 N_k^2\right) \tag{3.75}$$

$$J_{12} = J_{21} = \hat{c}Nd_x d_y \tag{3.76}$$

Defining

$$G \triangleq N(d_x^2 + d_y^2) \tag{3.77}$$

$$F \triangleq \frac{1}{2}\sum_{k=1}^{K} R_k^2 N_k^2\,, \tag{3.78}$$

the CRLB can be written as

$$CRLB = \frac{J_{11} + J_{22}}{J_{11}J_{22} - J_{12}J_{21}} = \frac{G + 2F}{\hat{c}(GF + F^2)}\,. \tag{3.79}$$

The partial derivative of the CRLB in (3.79) with respect to R_i is calculated as

$$\frac{\partial(CRLB)}{\partial(R_i)} = -\frac{G^2\frac{\partial F}{\partial R_i} + 2GF\frac{\partial F}{\partial R_i} + 2F^2\frac{\partial F}{\partial R_i}}{\hat{c}(GF + F^2)^2} \tag{3.80}$$

for $i \in \{1, \ldots, r\}$. Since $\dfrac{\partial F}{\partial R_i} = R_i N_i^2 > 0$, $F > 0$, $G > 0$ and $\hat{c} > 0$, the partial derivative of the CRLB in (3.80) is negative for all $R_i > 0$ and $i \in \{1, \ldots, r\}$. Since all the partial derivatives are negative, the CRLB is a monotone decreasing function of the radius R_i for each i. Hence, it is optimal to place the PDs at the boundary of the layout. ■

Proposition 1 states that in a uniform circular array configuration with $D \gg R$, placing the PDs to the maximum possible radius leads to the minimum CRLB in the case of identical and perpendicular PDs that are at the same known height, and this result holds for each uniform circular array in the presence of a superposition of multiple circular uniform arrays in the given VLC receiver. For example, considering scenarios A, B, and C in Fig. 4.2, scenario C is optimal under the conditions in Proposition 1 in terms of minimizing the CRLB since it employs the maximum radius for each PD.

Table 3.1: List of trigonometric summations for ψ_n in (3.20).

Expression 1	**Expression 2**	**Result**
$\sum_n \cos\psi_n$	$\sum_n \sin\psi_n$	0
$\sum_n \cos^2\psi_n$	$\sum_n \sin^2\psi_n$	$N/2$
$\sum_n \cos\psi_n \sin\psi_n$	—	0
$\sum_n \cos^3\psi_n$	$\sum_n \sin^3\psi_n$	0
$\sum_n \cos^2\psi_n \sin\psi_n$	$\sum_n \cos\psi_n \sin^2\psi_n$	0
$\sum_n \cos^4\psi_n$	$\sum_n \sin^4\psi_n$	$3N/8$
$\sum_n \cos^3\psi_n \sin\psi_n$	$\sum_n \cos\psi_n \sin^3\psi_n$	0
$\sum_n \cos^2\psi_n \sin^2\psi_n$	—	$N/8$
$\sum_n \cos^5\psi_n$	$\sum_n \sin^5\psi_n$	0
$\sum_n \cos^4\psi_n \sin\psi_n$	$\sum_n \cos\psi_n \sin^4\psi_n$	0
$\sum_n \cos^3\psi_n \sin^2\psi_n$	$\sum_n \cos^2\psi_n \sin^3\psi_n$	0
$\sum_n \cos^6\psi_n$	$\sum_n \sin^6\psi_n$	$5N/16$
$\sum_n \cos^5\psi_n \sin\psi_n$	$\sum_n \cos\psi_n \sin^5\psi_n$	0
$\sum_n \cos^4\psi_n \sin^2\psi_n$	$\sum_n \cos^2\psi_n \sin^4\psi_n$	$N/16$
$\sum_n \cos^3\psi_n \sin^3\psi_n$	—	0

Chapter 4

Numerical Results

In this section, numerical evaluations of the CRLB expressions in Section 3 are performed in order to investigate the effects of different parameters on the performance of a SIMO VLP system in various scenarios. An empty room with dimensions $4\,\text{m.} \times 4\,\text{m.} \times 3\,\text{m.}$ is considered for the simulations, where $3\,\text{m.}$ corresponds to the height of the room. The Lambertian order is taken as $m = 1$ [32], and the LED transmitter is located at $\boldsymbol{l}_T = [0, 0, 3]^T$ (all in meters) with a transmit power of $P_T = 3\,\text{W}$, where the position coordinates are with respect to the center of the floor (i.e., the center of the floor is defined as the origin). To verify the closed form CRLB expressions in (3.33), (3.43), (3.51), and (3.57), which are derived based on the known height assumption, the VLC receiver is assumed to be placed on the top of an object (e.g., a robot) with a known height of $0.5\,\text{m.}$ (except for Section 4.5 in which the height is assumed to be unknown.) Thus, the position vector for the receiver is formed as $\boldsymbol{l}_R = [\boldsymbol{l}_R(1), \boldsymbol{l}_R(2), 0.5]^T$, where $-2\,\text{m.} \leq \boldsymbol{l}_R(1), \boldsymbol{l}_R(2) \leq 2\,\text{m.}$ The area of each PD is considered as $S_n = 25\,\text{mm}^2\ \forall n$, and the FOV of each PD is taken as $\theta_{\text{FOV},n} = 75^\circ\ \forall n$ [36]. In addition, [37, Eq. 6] and [38, Eq. 20] are employed to calculate the noise variances, σ_n^2. During those calculations, the parameters are chosen as in [37] (see Table I in [37]). While calculating the exact CRLB, the noise variances are obtained for each $\boldsymbol{l}_R$ separately since the noise variance also depends on the received RSS [37, 38]. (Throughout the room and for all possible elevation angles, the extreme values of σ^2 are calculated as

$\sigma^2_{max} = 1.8074 \times 10^{-16}$ and $\sigma^2_{min} = 1.8012 \times 10^{-16}$.) The number of PDs ($N$), the elevation angles for the PDs (β in Fig. 3.1-(a)) and the radius of the circular layout (R in Fig. 3.1-(b)) are specified in the following subsections. Then, the exact CRLB values are calculated via the expressions in (3.4)–(3.10), (3.13)–(3.17), or (3.29)–(3.32), and comparisons with the approximate CRLB expressions in (3.33), (3.43), (3.51), and (3.57) are performed.

4.1 Accuracy of Asymptotic Results

Equation (3.33) in Lemma 1 and (3.51) in Corollary 1 present approximate closed form CRLB expressions for the case of $D \ll R$ whereas (3.43) in Lemma 2 and (3.57) in Corollary 2 provide approximate CRLB formulas for the case of $D \gg R$. To investigate the accuracy of these approximations, numerical examples are presented in Fig. 4.1-(a) and (b), where the radius of the uniform circular layout is taken as $R = 0.15\,\text{m}$. and the number of PDs is specified as $N = 8$. Since the noise variances (σ_n^2's) at the PDs differ only slightly from each other at a given $\boldsymbol{l}_R$, σ^2 in (3.33), (3.43), (3.51), and (3.57) is replaced by the mean value of σ_n^2's at a particular position vector $\boldsymbol{l}_R$ while evaluating the approximate CRLB expressions. In Fig. 4.1-(a), the elevation angle of the PDs is taken as $\beta = 20^\circ$ and the CRLB is evaluated based on the approximations in Lemma 1 and Lemma 2 by locating the VLC receiver at various distances from the room center (origin) in a single direction (due to the symmetry). In addition, the exact 2-dimensional CRLB is evaluated via (3.29)–(3.32) and illustrated in the figure. In Fig. 4.1-(b), the PDs point up vertically (i.e. $\beta = 0^\circ$) and the CRLB expressions corresponding to the approximations in Corollary 1 and Corollary 2 are presented, together with the exact 2-dimensional CRLB. From the figures, it is observed that the approximations in Lemma 2 and Corollary 2 provide a close approximation to the exact CRLB for a wide range of distances since the condition of $D \gg R$ is satisfied in many positions in a practical setting. On the other hand, the approximations in Lemma 1 and Corollary 1 are quite accurate only around the point which is directly under the LED transmitter (i.e., $R \gg D$).

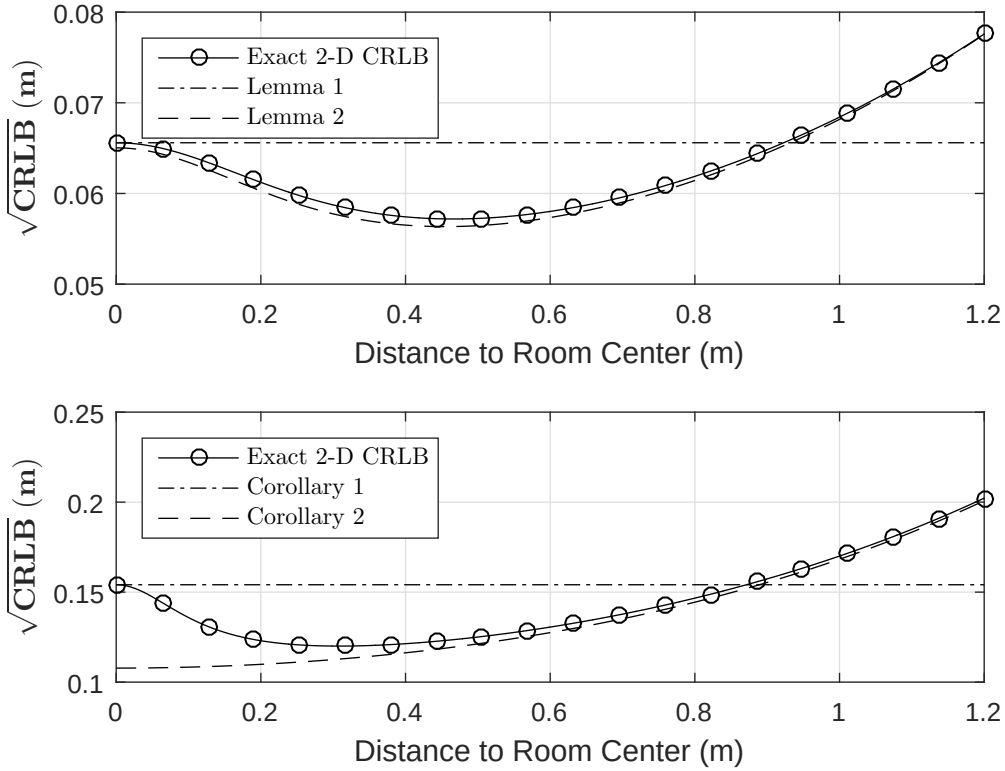

Figure 4.1: The approximate CRLB expressions compared with the exact CRLB. (a) Accuracy of Lemma 1 and Lemma 2. (b) Accuracy of Corollary 1 and Corollary 2.

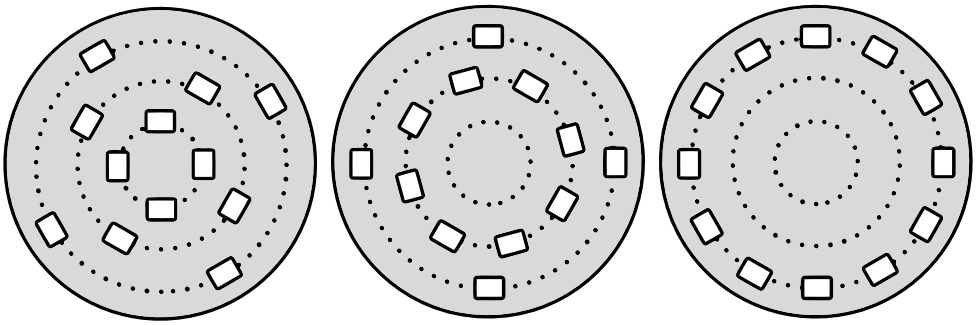

Figure 4.2: Three different scenarios with 12 PDs pointing up vertically and 3 circles with different radii.

4.2 Uniform Circular Layouts with Various Radii

Consider a configuration that is a superposition of multiple uniform circular layouts with various radii. Three different scenarios (A, B, and C) are investigated as shown in Fig. 4.2. In each scenario, 12 identical PDs are placed on 3 uniform circular layouts with radii R_1, R_2, and R_3, where each circle contains 4 PDs. Each PD points up vertically with an elevation angle of $\beta = 0$. In scenario A, the radii are set to $R_1 = 0.05\,\text{m.}$, $R_2 = 0.1\,\text{m.}$, and $R_3 = 0.15\,\text{m.}$, in scenario B, $R_1 = R_2 = 0.1\,\text{m.}$ and $R_3 = 0.15\,\text{m.}$, and in scenario C, $R_1 = R_2 = R_3 = 0.15\,\text{m.}$, where $0.15\,\text{m.}$ corresponds to the maximum possible value for the radius in the considered configuration. For these three scenarios, the exact CRLBs are calculated via (3.13)–(3.17) by placing the VLC receiver at various distances from the room center (origin). The results presented in Fig. 4.3 indicate that scenario C, in which all the PDs are located at the boundary of the layout, yields the minimum CRLBs. This is in accordance with Proposition 1, which states that the radii of all the circles should be set to the maximum possible value in order to minimize the CRLB for the case of $D \gg R$ (please also see the comments after Corollary 1). In fact, in this example, this result holds for all possible values of D. Since it is optimal to place the PDs at the boundary of the circular layout

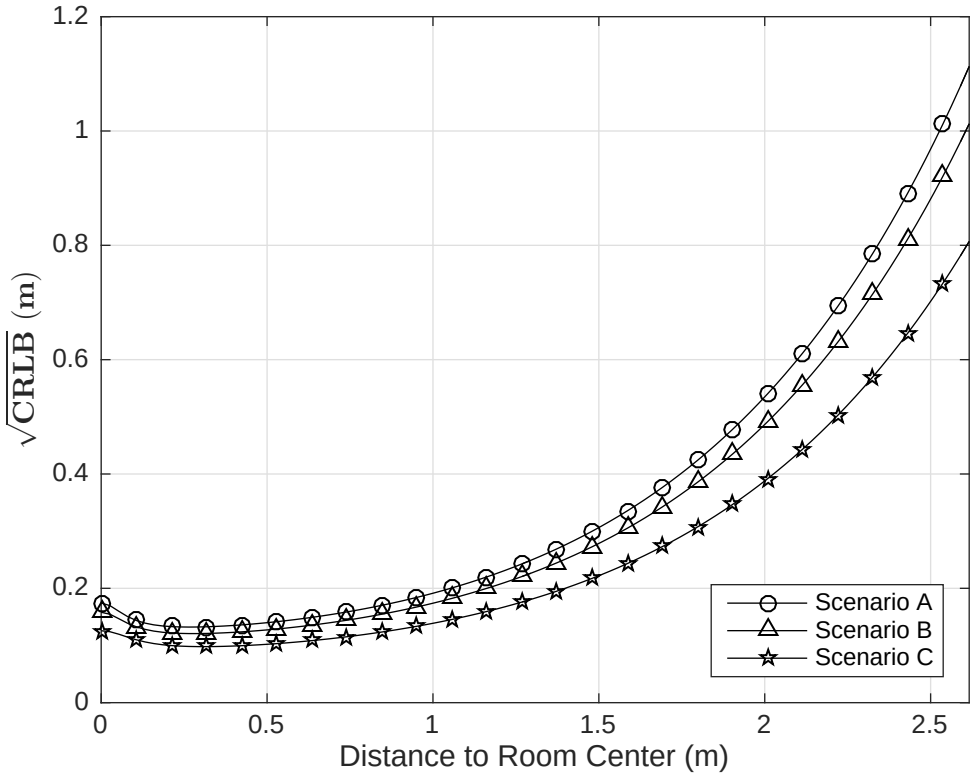

Figure 4.3: CRLB versus distance from the room center.

under certain conditions, scenario C is employed in the following subsections.

4.3 Elevated PDs at VLC Receiver

As investigated in [28], tilting the PDs placed on a uniform circular layout can provide certain benefits in some cases. In this part, the effects of tilting are investigated for the CRLB of a SIMO VLP system. In order to distinguish the impact of tilting on the CRLB, each PD is elevated by the same angle β, as illustrated in Fig. 3.1-(a). For the CRLB derivations in this study, the LED transmitter is assumed to lie within the FOV of each PD, as stated in Section 3. The conditions under which this assumption holds can be specified based on the

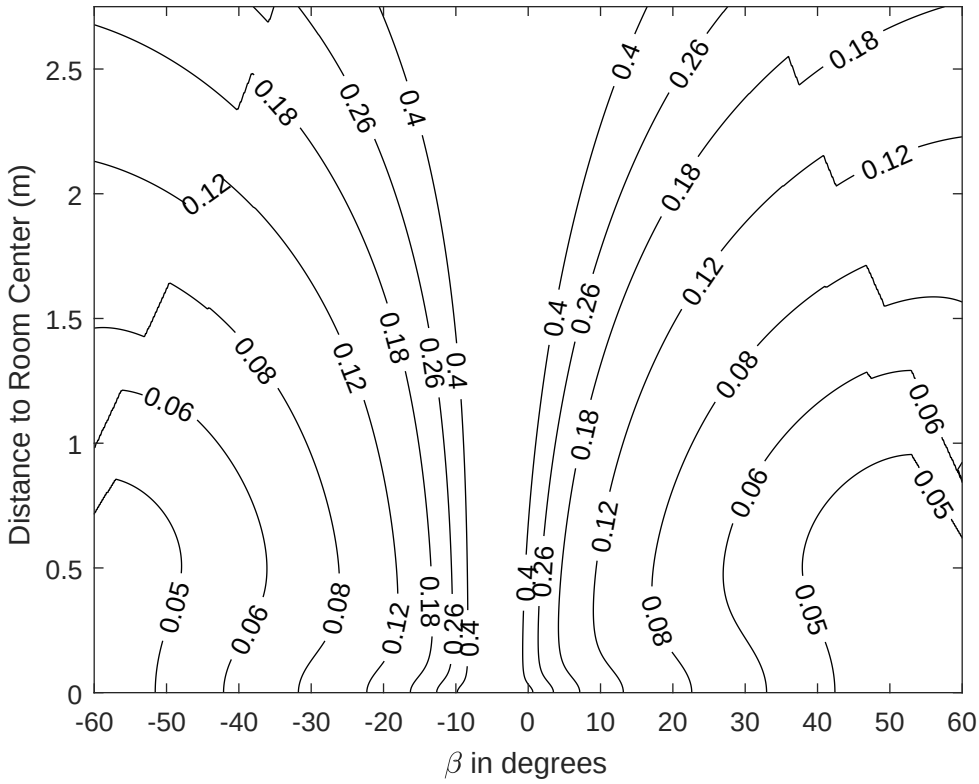

Figure 4.4: CRLB contour with respect to β and distance from the room center.

indicator function in (2.1) as follows:

$$\tan^{-1}\left(\frac{D-R}{H}\right) - \theta_{FOV} \leq \beta \leq \theta_{FOV} - \tan^{-1}\left(\frac{D+R}{H}\right) \tag{4.1}$$

In Fig. 4.4, the exact CRLBs are presented as a contour plot with respect to the elevation angle β and the distance from the room center. From the figure, the effects of the elevation angle of the PDs on the CRLB are observed for various distances from the room center. As β moves away from 0° in both positive and negative directions, the CRLB performance of the system improves. It is also noted that positive values of β yield slightly improved CRLB performance compared to their negative counterparts. This is due to the fact that when β is negative, the PDs facing the LED transmitter are further away from the room center. In addition, discontinuities are observed on the CRLB contours at some

β values where one or more PDs violate the condition in (4.1). In addition, the CRLB is observed to be a decreasing function of $\beta > 0$ in the region where (4.1) holds. Therefore, a reasonable choice for β at a given position of the VLC receiver can be obtained from (4.1) as

$$\beta_D^* = \theta_{FOV} - \tan^{-1}\left(\frac{D+R}{H}\right). \tag{4.2}$$

In order to guarantee that the LED transmitter lies within the FOV of each PD for all possible locations of the VLC receiver, β can be chosen as

$$\beta^* = \theta_{FOV} - \tan^{-1}\left(\frac{D_{\max}+R}{H}\right) \tag{4.3}$$

where $D_{\max}$ denotes the maximum distance from the room center, which is specified by the room geometry. In the considered scenario, $D_{\max} = 2\sqrt{2} - R\sqrt{2} = 2.758\,\text{m}.$ (where $R = 0.05\,\text{m}.$); hence, β^* turns out to be 26.68° since $H = 2.5\,\text{m}.$

4.4 Number of PDs and Layout Radius

The number of PDs at the VLC receiver, N, and the radius of the uniform circular layout, R, are important parameters of a SIMO VLP system that affect the localization accuracy. In this part, the average CRLB is calculated over the VLP system space, i.e., the plane on which the VLC receiver is located (at a height of $0.5\,\text{m}.$ from the floor) for various values of N and R. The PDs are tilted with an elevation angle of β_D^* for various values of the layout radius based on the expression in (4.2).

Fig. 4.5 illustrates the average CRLB (in meters) versus the number of PDs (N) for various values of the radius parameter R. In order to obtain the average CRLB, the CRLB values are calculated via (3.29)–(3.32) for multiple locations of the VLC receiver in the room, and the average of those CRLB values is computed as $CRLB_{avg}$. Then, the square root of $CRLB_{avg}$ is presented in Fig. 4.5. From the figure, it is observed that the average CRLB decreases as the number of PDs increases, as expected. Indeed, $\sqrt{CRLB_{avg}}$ is inversely proportional to the

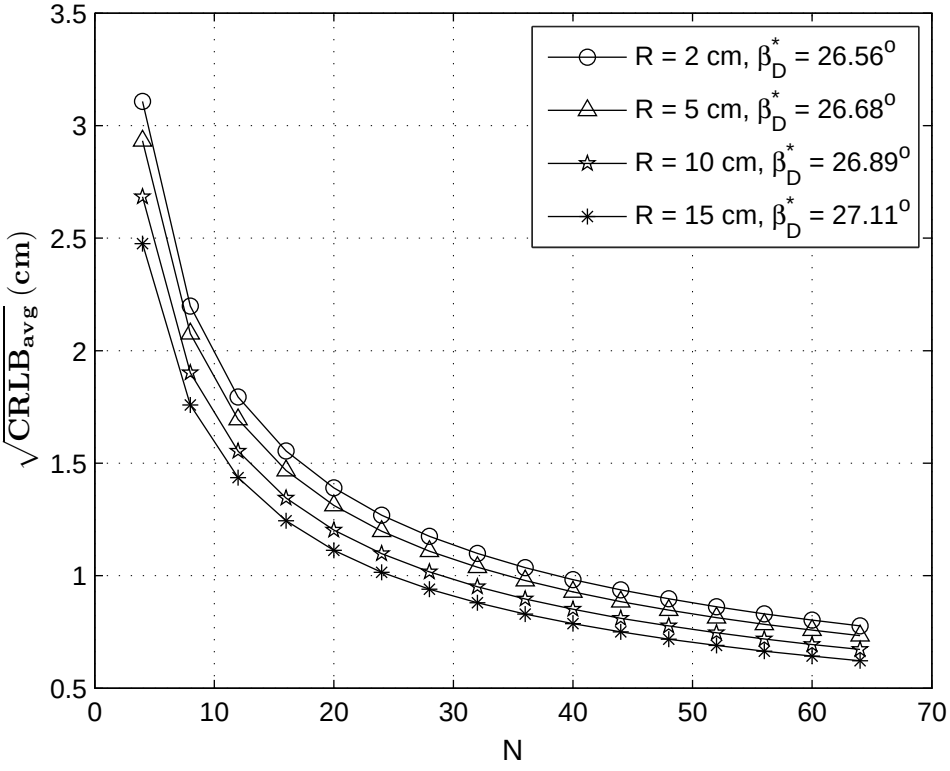

Figure 4.5: CRLB versus N for various radii.

square-root of N in accordance with Lemma 1 and Lemma 2 in this numerical example. In addition, the average CRLB is observed to decrease with the radius of the uniform circular layout. This is mainly due to the fact that more separated PDs in a uniform circular layout collect more information about the position. However, there exist practical limitations on the radius of the layout, which lead to a tradeoff between the localization performance and the VLC receiver size. From Fig. 4.5, it is also noted that an average CRLB of lower than 3.5 cm can be achieved for all configurations in the considered scenario. However, to achieve an average CRLB of 2 cm or lower, at least 12 PDs are required with a layout radius of at least $R = 2$ cm. A VLC receiver with a single PD that rotates along a circular path can be employed to realize the benefits of a high number of PDs. However, it requires additional circuitry for the rotation operation.

4.5 Maximum Likelihood Estimator (MLE)

Since the provided CRLB expressions present theoretical limits for the localization accuracy of SIMO VLP systems, it is important to compare them against the performance of some practical estimators. To that aim, the MLE is derived for the considered SIMO VLP system. The MLE is defined as

$$\hat{\boldsymbol{l}}_R = \arg\max_{\boldsymbol{l}_R} p(\boldsymbol{P}_R|\boldsymbol{l}_R) \tag{4.4}$$

where $\hat{\boldsymbol{l}}_R$ represents the MLE for the position of the VLC receiver, and the likelihood function, $p(\boldsymbol{P}_R|\boldsymbol{l}_R)$, is as presented in (3.1). The MLE in (4.4) reduces to following form based on (3.1):

$$\hat{\boldsymbol{l}}_R = \arg\min_{\boldsymbol{l}_R} \sum_{n=1}^{N} \frac{(P_{R_n} - f_n(\boldsymbol{l}_R))^2}{\sigma_n^2} \tag{4.5}$$

where P_{R_n} and $f_n(\boldsymbol{l}_R)$ are given by (2.1) and (3.2), respectively. To solve the optimization problem in (4.5), the *lsqnonlin* function of MATLAB is utilized by setting the initial point of the optimization to $[0, 0, 0]^T$. The MSE of the MLE is computed by considering 25000 realizations at each position of the VLC receiver, which is moved along the room diagonally. Also, the simulations are repeated for

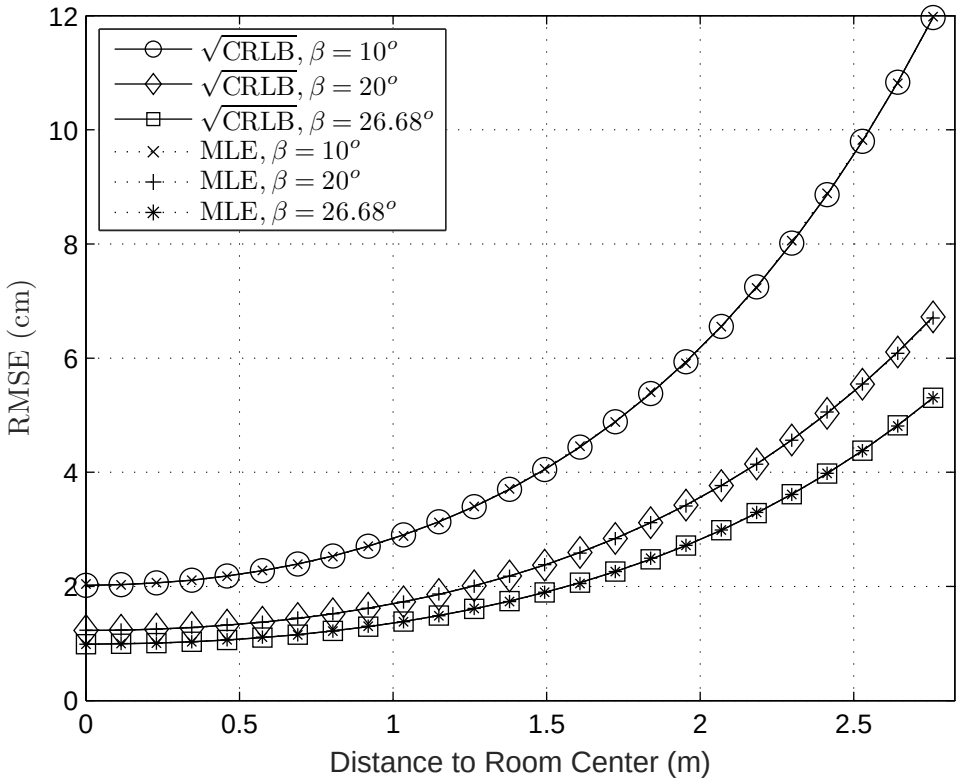

Figure 4.6: RMSE of MLE versus CRLB for different β values.

three different values of β. The number of PDs is set to $N = 12$ and the radius of the layout is taken as $R = 0.05$ in the simulations. In addition, the height of the VLC receiver is assumed to unknown in this case, and both the MLE and the CRLB are obtained for the 3-dimensional scenario (i.e., the CRLB is calculated via (3.4)–(3.10)). In Fig. 4.6, the root mean-squared errors (RMSEs) of the MLEs and the CRLBs are plotted versus the distance from the room center for various values of β. It is noted that the RMSEs of the MLEs achieve the CRLBs for all β values employed in the simulations. Hence, the MLE provides an effective estimation technique for localization in SIMO VLP systems.

Chapter 5

Concluding Remarks and Future Work

In this thesis, the RSS based CRLB has been derived for SIMO VLP systems for a generic three-dimensional scenario. In addition, specific CRLB expressions have been obtained for various scenarios in the presence of a known receiver height. In the first scenario, where all the PDs point upwards vertically (i.e., $\beta = 0$ in Fig. 3.1), the CRLB has been expressed in a closed form for a generic placement of the PDs. In the second scenario, the PDs are identical and located on a uniform circular layout, while in the last scenario, identical and perpendicular PDs have been employed along with the uniform circular layout. For these two scenarios, asymptotic analyses have been conducted, and the CRLB approximations have been obtained as compact closed form expressions for the cases of $D \ll R$ and $D \gg R$. Based on these theoretical results, the optimal configuration of the PDs at the VLC receiver has been determined under various conditions. In order to corroborate the theoretical results, numerical examples have been presented by considering different uniform circular layouts. Both the optimal PD configuration and the optimal elevation angle have been investigated in the examples. In addition, the MLE has been derived for the SIMO VLP system and compared against the CRLB. It has been observed that the MLE achieves a performance that is close to the CRLB; hence, it presents an effective estimation technique for

localization in SIMO VLP systems.

As future work, an experimental study for evaluating the MLE performance and comparing it against the CRLB will be conducted for SIMO VLP systems, considering various scenarios in terms of the number of PDs, elevation angles, and layouts. In addition, theoretical accuracy analysis for MIMO VLP systems is another important research direction.

Bibliography

[1] G. Mao and B. Fidan, *Localization Algorithms and Strategies for Wireless Sensor Networks*. Information Science Reference, 2009.

[2] K. Pahlavan and P. Krishnamurthy, *Principles of Wireless Access and Localization*. Wiley Desktop Editions, Wiley, 2013.

[3] E. Chan and G. Baciu, *Introduction to Wireless Localization: With iPhone SDK Examples*. Wiley, 2012.

[4] H. Liu, H. Darabi, P. Banerjee, and J. Liu, "Survey of wireless indoor positioning techniques and systems," *IEEE Transactions on Systems, Man, and Cybernetics, Part C (Applications and Reviews)*, vol. 37, pp. 1067–1080, Nov. 2007.

[5] Department of Defense, *GPS Standard Positioning Service (SPS) Performance Standard*. 4th ed., 2008.

[6] D. Dardari, E. Falletti, and M. Luise, *Satellite and Terrestrial Radio Positioning Techniques: A Signal Processing Perspective*. Oxford: Academic Press, 2012.

[7] M. Cypriani, F. Lassabe, P. Canalda, and F. Spies, "Wi-Fi-based indoor positioning: Basic techniques, hybrid algorithms and open software platform," in *International Conference on Indoor Positioning and Indoor Navigation (IPIN)*, Sep. 2010.

[8] Z. Sahinoglu, S. Gezici, and I. Guvenc, *Ultra-wideband Positioning Systems: Theoretical Limits, Ranging Algorithms, and Protocols*. New York: Cambridge University Press, 2008.

[9] J. Armstrong, Y. Sekercioglu, and A. Neild, "Visible light positioning: A roadmap for international standardization," *IEEE Communications Magazine*, vol. 51, pp. 68–73, Dec. 2013.

[10] M. A. Kashani and M. Kavehrad, "On the performance of single- and multi-carrie modulation schemes for indoor visible light communication systems," in *2014 IEEE Global Communications Conference*, pp. 2084–2089, Dec. 2014.

[11] H. Elgala, R. Mesleh, and H. Haas, "Indoor optical wireless communication: potential and state-of-the-art," *IEEE Communications Magazine*, vol. 49, pp. 56–62, Sep. 2011.

[12] J. Grubor, S. Randel, K. D. Langer, and J. W. Walewski, "Broadband information broadcasting using led-based interior lighting," *Journal of Lightwave Technology*, vol. 26, pp. 3883–3892, Dec 2008.

[13] D. Karunatilaka, F. Zafar, V. Kalavally, and R. Parthiban, "Led based indoor visible light communications: State of the art," *IEEE Communications Surveys Tutorials*, vol. 17, pp. 1649–1678, thirdquarter 2015.

[14] D. Ganti, W. Zhang, and M. Kavehrad, "VLC-based indoor positioning system with tracking capability using Kalman and particle filters," in *IEEE International Conference on Consumer Electronics (ICCE)*, pp. 476–477, Jan. 2014.

[15] L. Li, P. Hu, C. Peng, G. Shen, and F. Zhao, "Epsilon: A visible light based positioning system," in *11th USENIX Symposium on Networked Systems Design and Implementation*, (Seattle, WA), pp. 331–343, 2014.

[16] S. H. Yang, E. M. Jung, and S. K. Han, "Indoor location estimation based on LED visible light communication using multiple optical receivers," *IEEE Communications Letters*, vol. 17, pp. 1834–1837, Sep. 2013.

[17] Z. Zhou, M. Kavehrad, and P. Deng, "Indoor positioning algorithm using light-emitting diode visible light communications," *Optical Engineering*, vol. 51, no. 8, 2012.

[18] W. Zhang, M. I. S. Chowdhury, and M. Kavehrad, "Asynchronous indoor positioning system based on visible light communications," *Optical Engineering*, vol. 53, no. 4, pp. 045105–1–045105–9, 2014.

[19] H.-S. Kim, D.-R. Kim, S.-H. Yang, Y.-H. Son, and S.-K. Han, "An indoor visible light communication positioning system using a RF carrier allocation technique," *Journal of Lightwave Technology*, vol. 31, pp. 134–144, Jan. 2013.

[20] T. Q. Wang, Y. A. Sekercioglu, A. Neild, and J. Armstrong, "Position accuracy of time-of-arrival based ranging using visible light with application in indoor localization systems," *Journal of Lightwave Technology*, vol. 31, pp. 3302–3308, Oct. 2013.

[21] S.-Y. Jung, S. Hann, and C.-S. Park, "TDOA-based optical wireless indoor localization using LED ceiling lamps," *IEEE Transactions on Consumer Electronics*, vol. 57, pp. 1592–1597, Nov. 2011.

[22] M. Bilgi, A. Sevincer, M. Yuksel, and N. Pala, "Optical wireless localization," *Wireless Networks*, vol. 18, pp. 215–226, Feb. 2012.

[23] S.-H. Yang, H.-S. Kim, Y.-H. Son, and S.-K. Han, "Three-dimensional visible light indoor localization using AOA and RSS with multiple optical receivers," *Journal of Lightwave Technology*, vol. 32, pp. 2480–2485, July 2014.

[24] Y. S. Eroglu, I. Guvenc, N. Pala, and M. Yuksel, "AOA-based localization and tracking in multi-element VLC systems," in *IEEE 16th Annual Wireless and Microwave Technology Conference (WAMICON)*, Apr. 2015.

[25] A. Sahin, Y. S. Eroglu, I. Guvenc, N. Pala, and M. Yuksel, "Hybrid 3-D localization for visible light communication systems," *Journal of Lightwave Technology*, vol. 33, pp. 4589–4599, Nov. 2015.

[26] H. Steendam, T. Q. Wang, and J. Armstrong, "Cramer-Rao bound for indoor visible light positioning using an aperture-based angular-diversity receiver," in *IEEE International Conference on Communications (ICC)*, May 2016.

[27] L. Zeng, D. C. O'Brien, H. L. Minh, G. E. Faulkner, K. Lee, D. Jung, Y. Oh, and E. T. Won, "High data rate multiple input multiple output (MIMO) optical wireless communications using white led lighting," *IEEE Journal on Selected Areas in Communications*, vol. 27, pp. 1654–1662, Dec. 2009.

[28] A. Nuwanpriya, S. W. Ho, and C. S. Chen, "Indoor MIMO visible light communications: Novel angle diversity receivers for mobile users," *IEEE Journal on Selected Areas in Communications*, vol. 33, pp. 1780–1792, Sep. 2015.

[29] X. Zhang, J. Duan, Y. Fu, and A. Shi, "Theoretical accuracy analysis of indoor visible light communication positioning system based on received signal strength indicator," *Journal of Lightwave Technology*, vol. 32, pp. 4180–4186, Nov. 2014.

[30] M. F. Keskin and S. Gezici, "Comparative theoretical analysis of distance estimation in visible light positioning systems," *Journal of Lightwave Technology*, vol. 34, pp. 854–865, Feb. 2016.

[31] C. Amini, A. Taherpour, T. Khattab, and S. Gazor, "Theoretical accuracy analysis of indoor visible light communication positioning system based on time-of-arrival," in *IEEE Canadian Conference on Electrical and Computer Engineering (CCECE)*, May 2016.

[32] E. Gonendik and S. Gezici, "Fundamental limits on RSS based range estimation in visible light positioning systems," *IEEE Communications Letters*, vol. 19, pp. 2138–2141, Dec. 2015.

[33] M. F. Keskin, E. Gonendik, and S. Gezici, "Improved lower bounds for ranging in synchronous visible light positioning systems," *Journal of Lightwave Technology*, vol. 34, pp. 5496–5504, Dec. 2016.

[34] M. F. Keskin, S. Gezici, and O. Arikan, "Direct and two-step positioning in visible light systems," *IEEE Transactions on Communications*, under revision, 2017, Online: www.ee.bilkent.edu.tr/∼gezici/direct.pdf.

[35] H. V. Poor, *An Introduction to Signal Detection and Estimation*. New York: Springer-Verlag, 1994.

[36] Vishay Semiconductors, *Silicon PIN Photodiode*, 8 2011. Rev. 2.1.

[37] H. Ma, L. Lampe, and S. Hranilovic, "Coordinated broadcasting for multiuser indoor visible light communication systems," *IEEE Transactions on Communications*, vol. 63, pp. 3313–3324, Sep. 2015.

[38] T. Komine and M. Nakagawa, "Fundamental analysis for visible-light communication system using LED lights," *IEEE Transactions on Consumer Electronics*, vol. 50, pp. 100–107, Feb. 2004.